Lasers Med Sci (2015) 30:1335–1340
DOI 10.1007/s10103-015-1734-5

ORIGINAL ARTICLE

Highly accurate scattering spectra of strongly absorbing samples obtained using an integrating sphere system by considering the angular distribution of diffusely reflected light

D. Fukutomi · K. Ishii · K. Awazu

Received: 24 December 2014 / Accepted: 25 February 2015 / Published online: 15 March 2015

Abstract An integrating sphere system has been used to investigate the estimation error in the scattering coefficient for biological tissues. Since the angular distribution of diffusely reflected light from a sample may depend on the sample absorbance, leakage at the entrance port may affect estimates of the scattering coefficient based on measurement of diffuse reflectance. In the present study, the dependence of the angular distribution of the diffusely reflected light on the hemoglobin (Hb) concentration in a sample was investigated. Subsequently, the effect of the entrance port diameter on the error in the scattering coefficient estimated based on diffuse reflectance measurements was evaluated. For a biological tissue phantom, the angular reflectance distribution at a wavelength of 405 nm, at which strong absorption occurred, showed an increasing bias toward specular reflection as the Hb concentration was increased. No such concentration dependence was found at a wavelength of 664 nm, where the absorbance was low. In addition, it was found that the estimation error in the scattering coefficient was reduced for smaller entrance port diameters. Therefore, when attempting to determine the scattering coefficient for strongly absorbing samples, it is necessary to consider both the angular distribution of the diffusely reflected light and the optimal entrance port diameter.

D. Fukutomi · K. Ishii · K. Awazu (✉)
Graduate School of Engineering, Osaka University,
2-1 Yamadaoka, Suita, Osaka 565-0871, Japan
e-mail: awazu@see.eng.osaka-u.ac.jp

K. Awazu
Graduate School of Frontier Biosciences, Osaka University,
1-3 Yamadaoka, Suita, Osaka 565-0871, Japan

K. Awazu
The Center for Advanced Medical Engineering and Informatics,
Osaka University, 2-2 Yamadaoka, Suita, Osaka 565-0871, Japan

Keywords Integrating sphere · Inverse Monte Carlo simulation · Optical property · Scattering coefficient · Diffuse reflectance · Entrance port diameter

Introduction

Light propagation in biological tissues depends on optical properties such as the absorption coefficient μ_a, the scattering coefficient μ_s, the refractive index n, and the scattering anisotropy factor g. The ability to numerically model light propagation is important for obtaining quantitative information in medical diagnosis and therapy [1–3]. However, biological tissues are turbid media with both absorbing and scattering properties, and it is difficult in particular to analyze their light scattering behavior using conventional spectroscopy methods. Light attenuation due to scattering events cannot be described by simple formulas such as the Lambert-Beer law. There have therefore been many attempts to determine the optical properties of biological tissue using combined spectroscopic and simulation approaches [4–6].

One well-established method combines the use of an integrating sphere with inverse Monte Carlo (iMC) simulations, and there have been many reports on the optical properties of biological tissues using this approach [7–9]. However, in some cases, erroneous values of μ_s were obtained [10, 11]. Based on our own investigations, the error in the estimated value of μ_s was significant at wavelengths where strong absorption occurred, such as the wavelength band in which hemoglobin (Hb) exhibits absorption peaks. The estimation error caused a local dip in the scattering spectrum, which became more significant as the Hb concentration increased [12]. In inhomogeneous turbid media such as biological tissues, the Mie and Rayleigh theories predict that the scattering spectrum should exhibit a monotonic change with wavelength [13]. Therefore, the local dip in the measured scattering spectrum can be considered to be an estimation error.

In a previous study, it was found that to avoid this distortion of the scattering spectrum, it was necessary to ensure that the diffuse reflectance R_d was accurately measured by the integrating sphere. Errors are thought to be introduced due to leakage of diffusely reflected light through the entrance port of the integrating sphere. This can be more significant for highly absorbing samples and leads to inaccurate values for μ_s.

The purpose of the present study was to develop a method for obtaining highly accurate scattering spectra for biological tissues. To investigate the source of the error, the dependence of the angular distribution of the diffusely reflected light on the Hb concentration was first determined. The influence of the entrance port diameter of the integrating sphere on the magnitude of the error was then evaluated.

Materials and methods

Measurement of the angular distribution of diffusely reflected light

Sample preparation

Biological tissue phantoms that imitate the optical properties of soft biological tissues were used. They contained Hb (H7379, Sigma-Aldrich, USA), a lipid emulsion (Intralipid 20 %, Terumo, Japan), and gelatin from porcine skin (G2500, Sigma-Aldrich, USA). The Hb was used as a light absorber with an absorption peak around 405 nm, and the lipid emulsion was used as a light scatterer. To produce the phantoms, aqueous Hb solutions with concentrations of 0.5, 1, 2, and 4 mg/mL were first prepared by serial dilution. To each of these solutions, 4 vol% lipid emulsion and 0.1 mg/mL gelatin were added. After sufficient mixing in hot water at 37 °C, the product was placed between two glass slides (S1112, Matsunami Glass Industries, Japan), and the sample thickness was adjusted to 0.5 mm using a spacer.

Optical setup

Figure 1a shows a schematic of the optical setup for measuring the angular distribution of diffusely reflected light. Continuous wave semiconductor lasers with wavelengths of 405 nm (VLM-500, Sumitomo Electric Industries, Japan) and 664 nm (UM1000 Dental_665, Jenoptik, Germany) were used. The laser beam was delivered via a multimode optical fiber (QP1000-1-VIS/NIR, Ocean Optics, USA) with a core diameter of 1000 μm, and the output beam was collimated using an achromatic lens with a focal length of 75 mm. The collimated beam was focused using a second achromatic lens with a focal length of 1000 mm, and the beam diameter was adjusted to 3 mm using an aperture. Finally, the beam was focused to a spot size of 2 mm on the sample surface using a biconvex lens with a focal length of 200 mm. The sample was located at the center of a rotary stage with a diameter of 300 mm (RBB12A, Thorlabs, USA). For both laser wavelengths, the irradiation power density was 1.7 mW/cm^2. The diffuse reflection intensity was measured within an angular range of −90° to 90° with respect to the incident light direction using a spectrometer (Maya2000-Pro, Ocean Optics, USA). The reflection light was delivered to the spectrometer via a multimode optical fiber with a core diameter of 1000 μm placed on the edge of the rotary stage. The distance between the irradiated spot on the sample surface and the detection fiber was 140 mm.

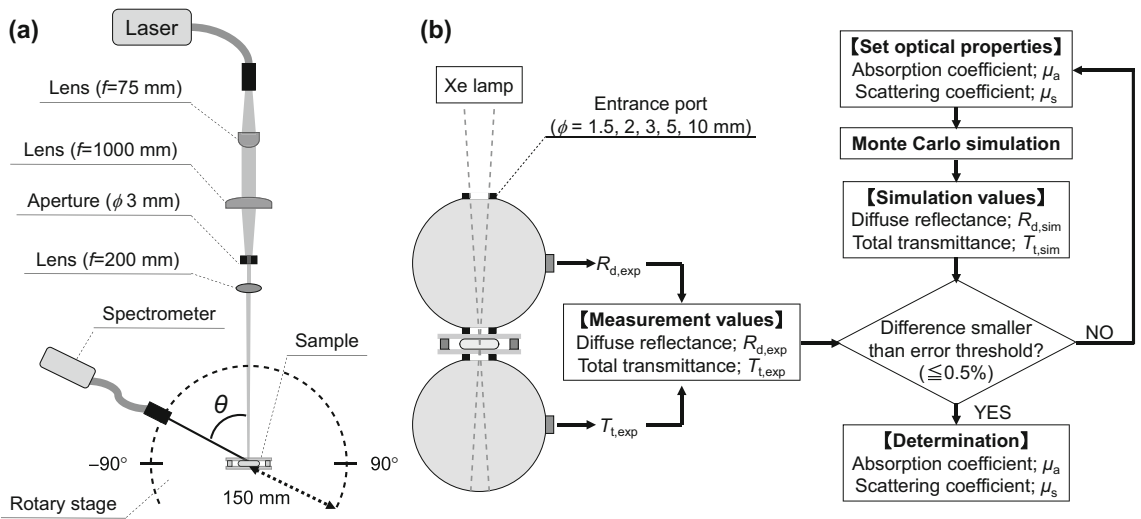

Fig. 1 **a** Experimental setup used for measuring the angular distribution of diffusely reflected light. **b** Experimental setup used for measuring diffuse reflectance and total transmittance, and the algorithm for the inverse Monte Carlo simulation

Determination of optical properties for different entrance port diameters

Sample preparation

Biological tissue phantoms with Hb concentrations of 0.5 and 2 mg/mL, prepared using the previously described method, were used during these measurements.

Optical setup

A double integrating sphere system was combined with iMC simulations in order to determine the optical properties of the samples (Fig. 1b). The sample was placed between two integrating spheres (3P-GPS-033-SL, Labsphere, USA), whose inner surfaces were coated with a diffusely reflective material, Spectralon™. The inner diameter of each sphere was 84 mm. The entrance port diameter for the integrating sphere used for diffuse reflectance measurements was adjusted to be 1.5, 2.0, 3.0, 5.0, or 10.0 mm. A xenon lamp (L2274 (GS), Hamamatsu, Japan) was employed as the light source. The pseudo-collimated beam was about 1 mm in diameter on the sample. The diffusely reflected light and total transmission light were multiply scattered in the integrating spheres, detected via multimode optical fibers with a core diameter of 600 μm (QP600-1-VIS-NIR, Ocean Optics, USA), and recorded as the R_d and the total transmittance T_t using a spectrometer (Maya2000 Pro, Ocean Optics, Japan) in the range 350 to 1000 nm.

Determination of optical properties

The iMC simulation, which was custom designed based on freely available Monte Carlo (MC) code [14, 15], was performed to determine μ_a and μ_s from the measured R_d and T_t values. The algorithm involved the following steps: (a) Initial values for μ_a and μ_s were estimated. (b) These were used to calculate simulated values for R_d and T_t using a Monte Carlo simulation for multilayer tissue. (c) The simulated R_d and T_t values were compared to the measured values. If they did not agree to within a predefined error margin (<0.5 %), new μ_a and μ_s values were used. (d) This procedure was repeated until the error threshold was achieved, and these μ_a and μ_s values were then accepted for the tissue. The calculations were performed for wavelengths in the range of 350 to 1000 nm. In the iMC calculations, the anisotropy factor and refractive index for the sample were fixed at 0.9 and 1.33, respectively.

Results

Angular distributions of diffusely reflected light

Figure 2a, b shows the angular distributions of the diffusely reflected light for the biological tissue phantoms for a wavelength of 405 and 664 nm, respectively, and for different Hb concentrations. In these figures, the radial direction represents the light intensity, and the circumferential direction represents the angle relative to the incident beam direction. The intensity values are normalized based on the maximum value for each measurement. Measurements were not performed in the range from −5° to +5° because of interference between the incident beam and the detection fiber. In Fig. 2a, it can be seen that the angular distribution shows a directional bias toward specular reflection with increasing Hb concentration. On the other hand, in Fig. 2b, no such dependence on the Hb concentration is observed.

Calculated optical properties for different entrance port diameters

Figure 3 shows scattering and absorption spectra for phantoms with Hb concentrations of 0.5 and 2 mg/mL for entrance port diameters of 1.5 to 10 mm. It can be seen that, at all wavelengths, μ_s increases with decreasing entrance port diameter.

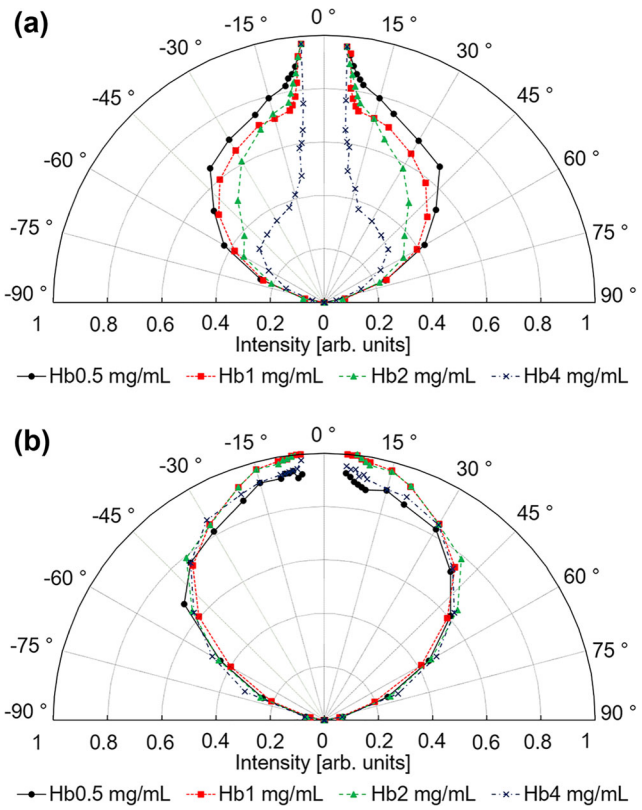

Fig. 2 Normalized angular distributions of diffusely reflected light for biological tissue phantoms at **a** 405 and **b** 664 nm

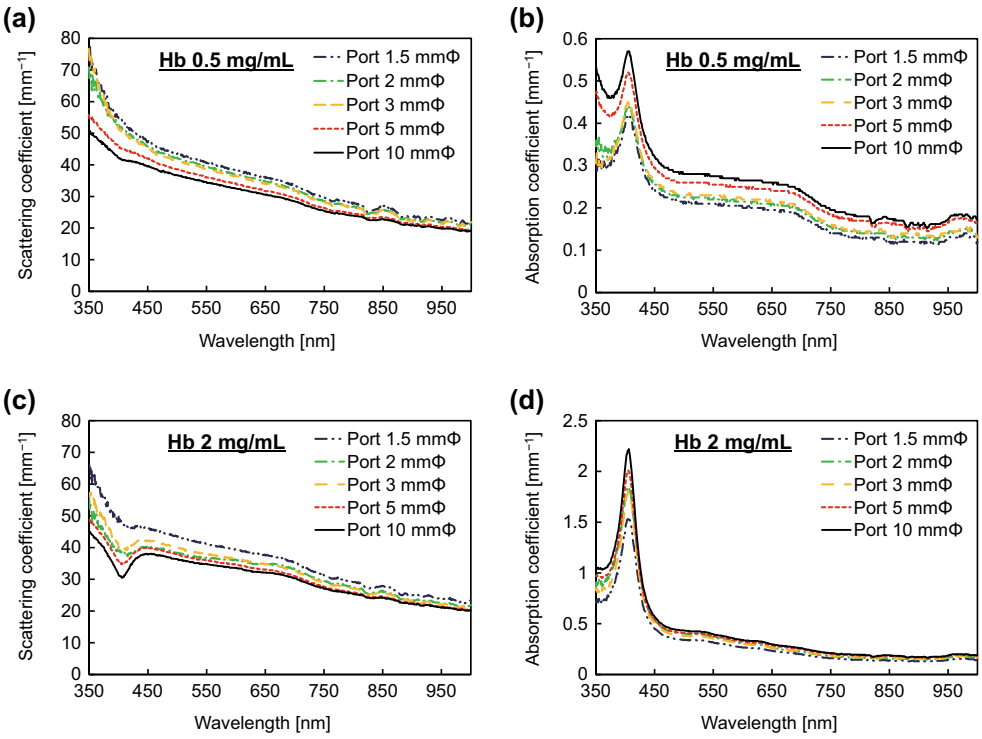

Fig. 3 Optical properties of biological tissue phantoms with obtaining using various entrance port diameters. **a**, **b** Scattering and absorption spectra, respectively, for a hemoglobin concentration of 0.5 mg/mL. **c**, **d** Scattering and absorption spectra, respectively, for a hemoglobin concentration of 2 mg/mL

This is particularly true at short wavelengths from 350 to 450 nm. Also, the local dip in the μ_s spectrum that occurs in this wavelength range, which is due to an error in the estimated values, disappears for small entrance port diameters. On the other hand, at all wavelengths, μ_a decreases with decreasing entrance port diameter.

Discussion

The angular distribution of the diffusely reflected light was found to depend on the absorbance of the sample. One reason for this is considered to be that light propagation and diffusion depend on the absorbance of tissue. Figure 4a, b shows the results of an MC simulation of light propagation using the optical properties of a biological tissue phantom with a Hb concentration of 2 mg/mL at a wavelength of 405 and 664 nm, respectively, and for an entrance port diameter of 5 mm. In Fig. 4a, μ_a and μ_s were set to 2.0 and 34.7 mm^{-1}, respectively, to simulate for a strongly absorbing medium. The upper graph is a color-coded plot of the fluence (Fzr [J/cm^2]), and the lower graph shows the common logarithm of the fluence at the surface. Figure 4b shows the situation for a weakly absorbing medium, where μ_a and μ_s were set to 0.3

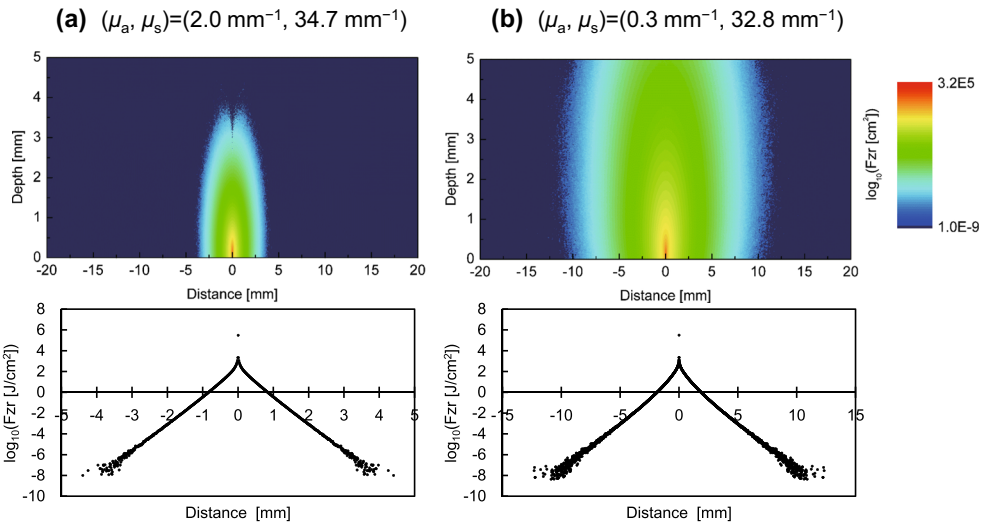

Fig. 4 MC simulation results for light propagation (*upper*) and surface fluence (*lower*). **a** (μ_a, μ_s) = (2.0 mm^{-1}, 34.7 mm^{-1}) and **b** (μ_a, μ_s) = (0.3 mm^{-1}, 32.8 mm^{-1})

and 32.8 mm^{-1}, respectively. From these results, it is clear that the light propagation path is narrower in a strongly absorbing medium. This suggests that the region where diffusely reflected photons are present is also narrow.

Another reason for the dependence of the angular distribution of the diffusely reflected light on the sample absorbance may be anomalous dispersion of n. There have been some reports that n exhibited a dependence on wavelength and absorbance, and in a strongly absorbing medium, such anomalous dispersion occurred at the center of the absorption peak [16–18]. This gave rise to a distortion in the specular reflectance spectrum in the form of a first derivative [18]. In the present study, it is thought that the specular component of the measured diffuse reflectance spectrum underwent a similar distortion due to anomalous dispersion of n in the high-absorption wavelength band for Hb. Thus, the angular distribution of the diffusely reflected light showed a directional bias toward specular reflection under high absorbance conditions.

Figure 5a shows the difference between R_d values measured using different entrance port diameters and that for an entrance port diameter of 10 mm, at a Hb concentration of 2 mg/mL and a wavelength of 405 nm. Although these differences are very small, they give rise to the large changes in the optical properties seen in Fig. 3. For an integrating sphere, the accuracy to which R_d can be measured was found to depend on the entrance port diameter. It is thought that reducing the diameter prevents diffusely reflected light from leaking, thereby improving the estimation of μ_s.

As described above, the estimation error in μ_s was improved by reducing the entrance port diameter. In order to allow a quantitative comparison, the estimation error is expressed as a "misfit ratio [%]" and is given in Eq. (1) below.

$$\text{misfit ratio} = \left(1 - \frac{\text{experimental value}}{\text{theoretical value}}\right) \times 100 \quad (1)$$

The misfit ratio for a biological tissue phantom with a Hb concentration of 2 mg/mL was evaluated. In the scattering spectrum for an entrance port diameter of 1.5 mm, the erroneous local dip was comparatively small. Therefore, a moving average was used in order to reduce the noise, and a theoretical fit was performed using the scattering formula based on a wavelength power law shown in Eq. (2) [19].

$$\mu_s = A \times \lambda^{-p} \quad (2)$$

Here, A is an arbitrary constant, λ is the wavelength (nm), and p has a value of 0–4. If p=4, this corresponds to Rayleigh scattering. For smaller value of p, Mie scattering begins to dominate. The p value for the theoretical spectrum was 2.5. The constant A was determined by performing a least squares fit to the theoretical spectrum in the wavelength range of 550 to 700 nm. The theoretical spectrum was determined by a trial-and-error approach, comparing its slope for different p values

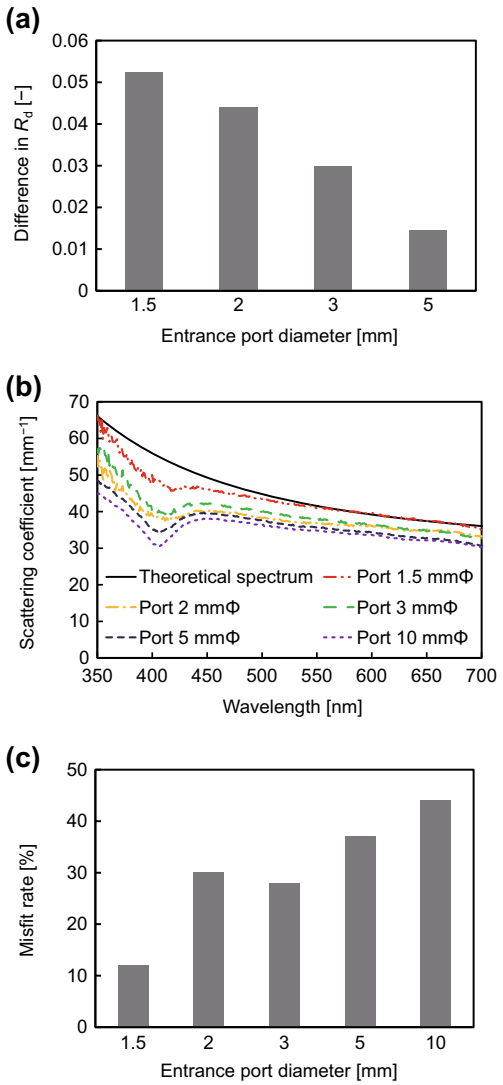

Fig. 5 **a** Difference between R_d values determined at various entrance port diameters for a Hb concentration of 2 mg/mL at a wavelength of 405 nm and that for a conventional entrance port diameter of 10 mm. **b** Calculated and theoretical scattering spectra for a Hb concentration of 2 mg/mL. **c** Misfit ratio at 405 nm

to that of the moving-averaged spectrum in the shorter wavelength range from 350 to 550 nm. Figure 5b shows scattering spectra in the range of 350 to 700 nm for phantoms with a Hb concentration of 2 mg/mL and various entrance port diameters. Here, the thick solid line represents the theoretical spectrum. Figure 5c shows the calculated misfit ratio at a wavelength of 405 nm. The misfit ratio clearly decreased with decreasing entrance port diameter, being 44.0 and 12.1 % for a diameter of 10 and 1.5 mm, respectively.

Although in the present study, g and n were fixed, in reality, they exhibit a wavelength dependence and undergo irregular changes at wavelengths where strong absorption occurs [9, 16–18]. There have been few reports concerning the spectra of g and n in strongly absorbing media such as biological tissues. However, their wavelength dependences should be

considered when optical properties are being calculated. In our previous work [20], it was found that variations in n have little effect on μ_s. In contrast, however, μ_s is strongly affected by slight variations in g. Therefore, if the wavelength dependence of g is considered in the iMC simulations, more accurate calculation of the μ_s spectra can be expected.

Conclusion

The angular distribution of diffusely reflected light from Hb-containing samples was evaluated at wavelengths of 405 and 664 nm, and a strong wavelength dependence was found. At 405 nm, the distribution showed a directional bias toward specular reflection with increasing Hb concentration. This bias was found to be responsible for the error in the estimated value of μ_s. This error could be reduced by decreasing the diameter of the entrance port of the integrating sphere system. The results indicate that when attempting to determine μ_s for a strongly absorbing sample, it is important to consider the angular distribution of diffusely reflected light and optimize the entrance port diameter.

References

1. Cheong W, Prahl SA, Welch AJ (1990) A review of optical properties of biological tissues. IEEE J Quantum Electron 26(12):2166–2185
2. Hourdakis CJ, Penis A (1995) A Monte Carlo estimation of tissue optical properties for use in laser dosimetry. Phys Med Biol 40:351–364
3. Ritz JP, Roggan A, Isbert C, Muller G, Buhr HJ, Germer CT (2001) Optical properties of native and coagulated porcine liver tissue between 400 and 2400 nm. Laser Surg Med 29:205–212
4. Doornbos RMP, Lang R, Aalders MC, Cross FW, Sterenborg HJCM (1999) The determination of in vivo human tissue optical properties and absolute chromophore concentrations using spatially resolved steady-state diffuse reflectance spectroscopy. Phys Med Biol 44: 967–981
5. Roggan A, Friebel M, Dorschel K, Hahn A, Muller G (1999) Optical properties of circulating human blood in the wavelength range 400–2500 nm. J Biomed Opt 4:36–46
6. Troy TL, Thennadil SN (2001) Optical properties of human skin in the near infrared wavelength range of 1000 to 2200 nm. J Biomed Opt 6:167–176
7. Yust BG, Mimun LC, Sardar DK (2012) Optical absorption and scattering of bovine cornea, lens, and retina in the near-infrared region. Lasers Med Sci 27:413–422
8. Yaroslavsky AN, Schulze PC, Yaroslavsky IV, Schober R, Ulrich F, Schwarzmaier H-J (2002) Optical properties of selected native and coagulated human brain tissues in vitro in the visible and near infrared spectral range. Phys Med Biol 47:2059–2073
9. Friebel M, Roggan A, Muller G, Meinke M (2006) Determination of optical properties of human blood in the spectral range 250 to 1100 nm using Monte Carlo simulations with hematocrit-dependent effective scattering phase functions. J Biomed Opt 11:034021
10. Salomatina E, Jiang B, Novak J, Yaroslavsky AN (2006) Optical properties of normal and cancerous human skin in the visible and near-infrared spectral range. J Biomed Opt 11(6):064026
11. Meinke M, Muller G, Helfman J, Friebel M (2007) Optical properties of platelets and blood plasma and their influence on the optical behavior of whole blood in the visible to near infrared wavelength range. J Biomed Opt 12(1):014024
12. Terada T, Nanjo T, Honda N, Ishii K, Awazu K (2011) Error analysis of tissue optical properties determined by double-integrating sphere system and inverse Monte Carlo method. Proc SPIE 7897:78971W
13. Saidi IS, Jacques SL, Tittel FK (1995) Mie and Rayleigh modeling of visible-light scattering in neonatal skin. Appl Opt 34(31):7410–7418
14. Wang LH, Jacques SL, Zheng LQ (1995) MCML-Monte Carlo modeling of photon transport in multi-layered tissues. Comput Methods Prog Biomed 47:131–146
15. Oregon Medical Laser Center at Providence St. Vincent Medical Center http://omlc.ogi.edu/software/mc/
16. Sydoruk O, Zhernovaya O, Tuchin V, Douplik A (2012) Refractive index of solutions of human hemoglobin from the near-infrared to the ultraviolet range: Kramers-Kronig analysis. J Biomed Opt 17(11): 115002
17. Ding H, Lu JQ, Wooden WA, Kragel PJ, Hu X-H (2006) Refractive indices of human skin tissues at eight wavelengths and estimated dispersion relations between 300 and 1600 nm. Phys Med Biol 51: 1479–1489
18. Friebel M, Meinke M (2006) Model function to calculate the refractive index of native hemoglobin in the wavelength range of 250–1100 nm dependent on concentration. Appl Opt 45(12):2838–2842
19. Bashkatov AN, Genina EA, Kochubey VI, Tuchin VV (2005) Optical properties of human skin, subcutaneous and mucous tissues in the wavelength range from 400 to 2000 nm. J Phys D Appl Phys 38:2543–2555
20. Horibe T, Ishii K, Honda N, Awazu K (2013) Improvement of scattering coefficient estimation in inverse Monte Carlo calculation by considering wavelength dependence of refractive index and sample thickness. Proc CLSM 2013:2–11